Proceedings of the ASME 2024
International Design Engineering Technical Conferences and
Computers and Information in Engineering Conference
IDETC/CIE2024
August 25-28, 2024, Washington, DC

DETC2024-143546

PHYSICS-INFORMED DATA-DRIVEN APPROACHES TO ELECTRIC VEHICLE BATTERY STATE-OF-HEALTH PREDICTION: COMPARISON OF PARALLEL AND SERIES CONFIGURATIONS

Yixin Zhao
Environmental Engineering Sciences
University of Florida
Gainesville, FL, 32611
yixin.zhao@ufl.edu

Karl R. Haapala
Mechanical, Industrial, and Manufacturing Engineering
Oregon State University
Corvallis, OR, 97331
karl.haapala@oregonstate.edu

Arun Natarajan
Electrical Engineering and Computer Science
Oregon State University
Corvallis, OR, 97331
nataraja@eecs.oregonstate.edu

Sara Behdad*
Environmental Engineering Sciences
University of Florida
Gainesville, FL, 32611
sarabehdad@ufl.edu

ABSTRACT

Battery lifetime and reliability depend on accurate state-of-health (SOH) estimation, while complex degradation mechanisms and varying operating conditions strengthen this challenge. This study presents two physics-informed neural network (PINN) configurations, PINN-Parallel, and PINN-Series, designed to improve SOH prediction by combining an equivalent circuit model (ECM) with a long short-term memory (LSTM) network. PINN-Parallel process input data through parallel ECM and LSTM modules and combine their outputs for SOH estimation. On the other hand, the PINN-Series uses a sequential approach that feeds ECM-derived parameters into the LSTM network to supplement temporal data analysis with physics information. Both models utilize easily accessible voltage, current, and temperature data that match realistic battery monitoring constraints. Experimental evaluations show that PINN-Series outperforms the PINN-Parallel and the baseline LSTM model in accuracy and robustness. It also adapts well to different input conditions. This demonstrates that the simulated battery dynamic states from ECM increase the LSTM's ability to capture degradation patterns and improve the model's ability to explain complex battery behavior. However, the trade-off between the robustness and training efficiency of PINNs is also discussed. The research findings show the potential of PINN models (particularly the PINN-Series) in advancing battery management systems, but the required computational resources need to be considered.

Keywords: Lithium-ion battery; Electric vehicle; State of health; Physics-Informed Neural Network

1. INTRODUCTION

Electric vehicles (EVs) and their lithium-ion batteries are among the primary focuses of sustainable transportation [1]. As EVs become more widespread, understanding and predicting battery performance and lifespan is critical to vehicle reliability and lifecycle management [2]. The inevitable aging during usage results in a deterioration of the battery state of health (SOH) and makes the modeling of degradation critical for a reliable battery management system.

1.1 Related Work

There are two broad approaches to building the battery degradation model for battery in-use status prediction and diagnosis: the physics-based and the data-driven approach. The physics-based method can be further divided into electrochemical models and equivalent circuit models (ECM). The electrochemical model describes the degradation mechanisms of a battery based on its specific material properties

and operating parameters [3]. For example, the most widely adopted pseudo-two-dimensional (P2D) model offers a thorough examination of the thermal energy balance, mass balances, charge balances, and kinetics of electrochemical reactions within the cell [4]. However, the P2D model usually includes solving a set of tightly coupled differential equations [5]. The process is too complex and slow to be used for real-time management of in-use batteries. In order to reduce the computational demand, simplified versions of the P2D model have been developed, such as the single particle model [6]. For fast simulation, this model did not consider the variations in the electrolyte concentration and the potential [7]. Hence, it is not applicable to the simulation of high discharge rate cases, which is one of the required characteristics of EV batteries.

The ECM simulates the electrical behavior of a battery by using a combination of circuit elements [8,9]. A standard ECM typically employs an RC network, which consists of resistors and capacitors arranged in parallel, to replicate the dynamic behaviors of the battery [10]. Similar to the electrochemical model, it captures the dynamics of battery current and voltage in a physically explainable way. But ECM has a simpler structure and governing equations and therefore offers faster computation. Different orders of ECMs are shown to be effective in simulating batteries and can be used for SOH prediction [9]. The common ECMs include the Rint model, RC model, Thevenin model, Dual-Polarization model, and Partnership for a New Generation of Vehicles (PNGV) model [11]. However, the identification of ECM parameters based on underlying experimental data tends to limit its application [5]. For example, a parameterized ECM that assumes low C-rate charging and discharging of batteries at ambient temperature may not be applicable to another scenario.

On the other hand, the data-driven model can utilize large datasets to train the model to capture various operating parameters and battery responses. Among others, deep learning models have been evidenced to accurately simulate complex nonlinear battery systems, such as the long short-term memory (LSTM) network. This indicates that the physical-based model in practice can be improved with a data-driven approach to compensate for its incompleteness or inflexibility [12]. In addition, the interpretability of the physical model can be protected and provides the opportunity to reduce the demand for large amounts of training data. The integrated model shows promise in addressing the uncertainty of aging conditions [13], thermal management [14], and state of charge estimation [15,16].

Aykol et al. [17] categorized integration models for physical knowledge and deep learning into two broad categories: sequential combination of independent models and hybridized models. The first category does not require fundamental changes in the physics or the deep learning model. For instance, physical models can be used to generate synthetic data to train deep learning, while reducing the demand for experimental data collection [18]. The second category includes a hybrid architecture that embeds the physical or deep learning model in the other. The subsequent discussion mainly focuses on the hybridized model for predicting battery capacity or SOH.

To name several recent examples, Xu et al. [19] applied physical equations from a first-order Thevenin model to constrain and refine the predictions of an autoencoder. Models trained on battery discharge data can be used to predict SOH trajectories for the entire lifecycle of a test battery under similar operating conditions. Singh et al. [20] utilized Fick's law of diffusion from a single particle model to train the neural network, with inputs being a spatial vector of electrode particle radius along with a temporal vector for time. The simulated lithium solid-phase concentration is then used to calculate the state of charge, capacity, and SOH of the battery. Ye et al. [21] incorporated the monotonous relationship between the peak of the incremental capacity curve and the SOH into a neural network. Their enhanced model shows improvement in prediction accuracy. Fu et al. [22] integrated a second-order ECM into the recurrent neural network to estimate battery discharge profiles. The ohmic resistances identified from this hybrid network can be used to approximate SOH based on the assumed linear relationship. Lin et al. [23] proposed a framework that combines ECM with deep learning to extract key parameters from electrochemical impedance spectroscopy, reflecting the internal states of the battery. The multi-task learning and physical regularization are integrated to achieve more accurate and interpretable estimation results.

1.2 Problem Statement

Previous research has shown the promise of combining physics with data-driven models to improve battery SOH estimation. However, there are more directions to be explored in this emerging area. It is important to note that many hybrid models require pre-defined or known parameters based on physical (especially electrochemical) models. This requirement limits the generalizability of plain data-driven models to different battery chemistries and operating conditions. In addition, the incorporation of certain physical laws improves the interpretability of the model. However, this might also require additional battery testing, such as electrochemical impedance spectroscopy and differential capacity analysis, which are not easily accessible during routine battery operations. Moreover, discussions on the comparison of training costs between hybrid models and purely data-driven approaches are uncommon.

To address these gaps, this study develops Physics-Informed Neural Network (PINN) frameworks for SOH estimation that consider robustness and practicality. The PINNs are designed to process easily accessible voltage, current, and temperature measurements without presetting physical parameters, thus increasing the model's application in practice. The hybrid architecture integrates physics information from the ECM and LSTM network. The ECM is chosen because its governing equations are simple and fewer parameters to be processed by PINNs. Also, the good performance of LSTM in battery condition diagnosis shows its potential to capture complex temporal relationships. This paper comparatively explores parallel and sequential configurations of ECM and LSTM components, referred to as PINN-Parallel and PINN-Series, respectively. The parameters of both components are trainable

and optimized by a custom loss function that contains physical constraints. During the evaluation phase, an independent LSTM model is used as a baseline to comparatively analyze the accuracy, robustness, and computational efficiency of each model.

The rest of this paper is organized as follows. Section 2 includes the description of the dataset and structure of PINN frameworks. Section 3 provides details on the experiment implementation and a comparative analysis of these models in different scenarios. Finally, Section 4 summarizes the work and future research perspectives.

2. METHODOLOGY

2.1 Data Description and SOH Definition

This study used data from the NASA Ames Diagnostic Center of Excellence database, that was measured on commercial lithium-ion rechargeable batteries under controlled experimental conditions [24]. Data from batteries 0005, 0006, 0007, and 0018 were selected for the experiment, which have the same chemical composition. The process of data collection included repeated charging and discharging cycles of the batteries at room temperature. The initial temperature of each battery was around 24°C. The batteries were charged at a constant current of 1.5 A until each cell reached a voltage of 4.2 V. The charging mode was then switched to constant voltage until the charging current was reduced to 20 mA. Discharging was performed at a constant current of 2 A, with cutoff voltages of 2.7 V, 2.5 V, 2.2 V, and 2.5 V for batteries 0005, 0006, 0007, and 0018, respectively. The dataset does not mention the rest periods between cycles when describing the experiment process. The voltage (V), current (I), and temperature (T) signals were recorded at a frequency of 10 Hz throughout the charge/discharge cycle. The batteries have shown significant aging, which is mainly due to repeated cycling. The experiments were completed once the battery capacity was reduced by 30%, which indicated that the battery had reached its end-of-life. The capacity changes observed in the four target batteries are presented in Figure 1. Although all batteries have the same nominal capacity of 2.0 Ah, variations in their initial states and minor manufacturing differences can lead to different initial capacities at the start of the experiments. The four batteries also have different degradation trajectories due to differences in depth of discharge and intrinsic variability. This uncertainty in reflecting actual use is addressed by the proposed model.

After completing a full charge/discharge cycle, the cycle number count of the battery is incremented by one. The data utilized as input for the models in this study are time-series signals of voltage, current, and temperature during the charging phase of each battery cycle. These are considered measurable parameters, easily accessible during battery operation. Corresponding to these three charging profiles, the model's targeted output is the battery's SOH for the current cycle. The SOH is defined by the ratio of the nominal capacity to the releasable capacity, and it is displayed as:

$$SOH(\%) = \frac{Q_{max}}{Q_{norm}} \times 100\% \quad (1)$$

where Q_{max} is the maximal available capacity at the current cycle, and Q_{norm} is the nominal capacity given by the manufacturer.

Due to the varying charging time for different cycle, the V, I, T data also show different lengths. In the data preprocessing, each V, I, T curve is interpolated to produce a uniform series of 100 equidistant points. This approach preserves the time-series nature of the data while normalizing the length of the input signal. It also reduces the number of raw data points and decreases the computational load.

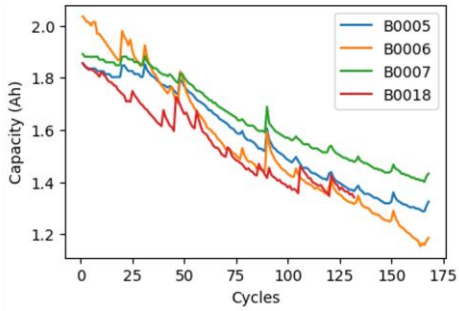

FIGURE 1: CAPACITY DEGRADATION OF BATTERIES

2.2 Equivalent Circuit Model Embedded in PINN

The proposed PINN models in this study embed the ECM into the LSTM framework. The ECM and electrochemical models are two classical physics-based models for providing information about the battery's internal processes. Compared to the electrochemical model, the ECM is easier to parameterize and verify but is also effective in predicting battery states [25]. There are multiple options for ECMs that can be embedded for simulating the battery's internal dynamics, such as the common ECMs mentioned in Section 1.1. However, in order to minimize the reliance on prior physical parameters and additional battery tests, the unknown parameters in the ECM are all represented by the MLP in the proposed framework. A complex ECM increases the difficulty of the neural network parameter optimization process and requires more computational cost [26]. For the consideration of the lightweight structure of the hybrid model, the basic Rint model is selected for the experiment. The schematic representations of the Rint model are shown in Figure 2 and Equation (2). Although the structure is simple, the Rint model's ability to increase the performance of a conventional data-driven model is demonstrated in the results section.

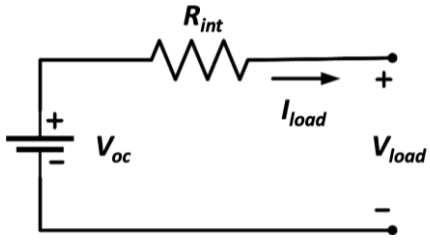

FIGURE 2: SCHEMATIC REPRESENTATION OF THE RINT MODEL

$$V = V_{OC} - I \cdot R_{int} \quad (2)$$

where V and I denote the battery terminal voltage and load current, V_{OC} indicates the open circuit voltage, and R_{int} represents ohmic resistance.

In the Rint model, terminal voltage and load current reflect the direct electrical response of the battery under load conditions. The equation essentially captures how the battery's V varies with the I, R_{int}, and V_{OC}. During the battery operation, V and I are accessible and measurable parameters. While V_{OC} and R_{int} are critical to understanding the battery's internal state, they cannot be directly measured. In particular, internal resistance is a key parameter that can characterize battery degradation. Therefore, V and I can be employed as input in the ECM component to infer these internal parameters. Although the effect of temperature is ignored in the Rint model, including easily accessible temperature data as input increases the reliability of the ECM component.

2.3 Long Short-Term Memory Module in PINN

The LSTM module is designed to capture temporal dependencies within the time-series data of battery charging cycles. The LSTM can remember long-term dependencies and mitigate the vanishing gradient problem commonly associated with traditional recurrent neural networks [27]. By processing the input time series data using a sliding window, LSTM can have the memory of historical information. For battery application, a sliding window would consist of a series of input signals across multiple battery cycles. The window "slides" forward in time, moving one or more timesteps after each operation, depending on the stride. The signal vector X at battery cycle t can be shown as:

$$X_t = \begin{pmatrix} signal_{1,1}(t) & signal_{1,2}(t) & \cdots & signal_{1,m}(t) \\ signal_{2,1}(t) & signal_{2,2}(t) & \cdots & signal_{2,m}(t) \\ \cdots & \cdots & \cdots & \cdots \\ signal_{y,1}(t) & signal_{y,1}(t) & \cdots & signal_{y,m}(t) \end{pmatrix} \quad (3)$$

where $signal_{i,j}(t)$ is the value of i^{th} input signal for the j^{th} time point within battery cycle t, the signal could be voltage, current, and temperature profiles during charging.

A window SW_t of size w containing the signal vectors over the previous $w-1$ cycles and the current cycle *t*, where:

$$SW_t = [X_{t-w+1}, X_{t-w+2}, \dots, X_t] \quad (4)$$

Each of these subsequences is then fed into the LSTM network, and the network learns from the temporal structure within each window. The LSTM recurrence equations at each time step t are given in Equation (5) to Equation (10) [28,29]:

$$i_t = \sigma\left(W_i \cdot [h_{t-1}, SW_t] + b_i\right) \quad (5)$$

$$f_t = \sigma\left(W_f \cdot [h_{t-1}, SW_t] + b_f\right) \quad (6)$$

$$o_t = \sigma\left(W_o \cdot [h_{t-1}, SW_t] + b_o\right) \quad (7)$$

$$g_t = \tanh\left(W_g \cdot [h_{t-1}, SW_t] + b_g\right) \quad (8)$$

$$c_t = f_t \cdot c_{t-1} + i_t \cdot g_t \quad (9)$$

$$h_t = o_t \cdot \tanh(c_t) \quad (10)$$

where i_t, f_t, o_t, g_t are input gate, forget gate, output gate, and candidate cell state, respectively; σ and $tanh$ are activation functions; W_i, W_f, W_o, W_g are the weight matrices; b_i, b_f, b_o, b_g are the bias vectors; h_t and c_t are hidden states and cell states that update over time.

The LSTM processes the time-series battery cycle and updates its cell and hidden states at each timestep within the window. The final output of the LSTM module, h_t, serves as a representation of the learned temporal information of window SW_t.

2.4 Proposed PINN framework

This study presents two PINN architectures, PINN-Parallel and PINN-Series, as shown in Figure 3. Both structures consist of an Equivalent Circuit Model (ECM) module, a Long Short-Term Memory (LSTM) module, and a customized loss function embedded with physical constraints. The main difference between the two is the layout: the ECM and LSTM modules are operated in parallel in PINN-Parallel, whereas they are sequentially connected in PINN-Series.

The ECM module is constructed based on the selected Rint model from Section 2.2. Its operational principle involves using a Multilayer Perceptron (MLP) network to estimate the battery's internal states from the dataset's voltage, current, and temperature signals. Due to the dynamic nature of the ECM, the module can process input time-series data of battery V, I, and T for each cycle. Therefore, the ECM component generates corresponding time-series estimates for the open-circuit voltage (V_{OC}) and internal resistance (R_{int}).

To validate the internal state estimation, two physical constraints are required on the ECM module. First, the predicted values of V_{OC} and R_{int} should not be negative. Second, due to the nonlinear relationship between the two internal parameters and the battery's state of charge, the ECM outputs are required to show temporal continuity. Large discrepancies between parameters at consecutive time points are penalized to maintain this continuity.

The LSTM module is capable of understanding temporal information within the batter cycling data, as described in Section 2.3. The sliding window helps the LSTM consider the target cycle as well as a predefined length of historical data. This provides the network with a richer framework for making predictions.

In the PINN-Parallel model, both the ECM and LSTM modules receive input signals $\{V, I, T\}$ from the battery charging process. The ECM block only processes signals on target battery cycle t and outputs the corresponding $[V_{OC}(t), R_{int}(t)]$. The LSTM receives a sliding window of

$[V(t), I(t), T(t)]$ over multiple cycles, where each window includes data from the target cycle and a predefined number of past cycles (Equation 4). The LSTM processes this window to output a final hidden state containing learned temporal information. The final dense layer of PINN-Parallel combines outputs from both the ECM and LSTM to predict the SOH for the target cycle.

In the PINN-Series model, the ECM first processes a sliding window of input signals $[V(t), I(t), T(t)]$, with its outputs fed into the LSTM along with the original signals. Therefore, the LSTM processes a $[V(t), I(t), T(t), V_{OC}(t), R_{int}(t)]$ sliding window over multiple cycles. The final dense layer takes the hidden state vector that captures both the temporal patterns in the original signals and the dynamics reflected in the ECM outputs to predict the SOH.

The loss function designed as the optimization objective for both frameworks is a composite of three parts, integrating the final SOH prediction accuracy in Equation (11), errors from the ECM predictions in Equation (12) (13), and the continuity of ECM parameters in Equation (14). To mathematically describe the three parts of loss:

$$Loss_{SOH} = \frac{1}{N}\sum_{t=1}^{N}(SOH_{true}(t) - SOH_{pred}(t))^2 \quad (11)$$

where N is the number of battery cycles; $SOH_{true}(t)$, $SOH_{pred}(t)$ are true and predicted SOH for the t^{th} battery cycle.

$$Loss_{ECM} = \frac{1}{N}\sum_{t=1}^{N}\frac{1}{M}\sum_{i=1}^{M}(V_{true,i}(t) - V_{pred,i}(t))^2 \quad (12)$$

$$V_{pred,i}(t) = V_{OC,i}(t) - I_i(t) \cdot R_{int,i}(t) \quad (13)$$

where M is the number of voltage predictions within the t^{th} battery cycle; i indexes the time points within the t^{th} battery cycle; $V_{true,i}(t)$, $V_{pred,i}(t)$ are i^{th} true and predicted voltage; where $V_{pred,i}(t)$ is calculated based on i^{th} estimated $V_{OC}(t)$, $R_{int}(t)$, and known current $I(t)$ within the t^{th} battery cycle.

$$Loss_{cont} = \frac{1}{N}\sum_{t=1}^{N}\frac{1}{M-1}\sum_{i=1}^{M-1}(\left|V_{OC,i+1}(t) - V_{OC,i}(t)\right| + \left|R_{int,i+1}(t) - R_{int,i}(t)\right|) \quad (14)$$

where this component ensures smooth transitions for ECM parameters V_{OC} and R_{int} between consecutive time points i within t^{th} cycle, reflecting physical consistency.

The total loss is a weighted sum of these components:

$$Loss_{total} = \alpha\, Loss_{SOH} + \beta\, Loss_{ECM} + \gamma\, Loss_{cont} \quad (15)$$

where α, β, γ are weighting factors that balance the contributions of each loss component to the total loss.

The proposed PINN architectures offer a hybrid framework for predicting battery behavior. The loss function confirms that the PINN models accurately predict the battery's internal states and SOH while respecting the physical constraints and continuity inherent in the battery's behavior. Moreover, $Loss_{SOH}$ should be given higher weight relative to the other losses to emphasize its importance in the framework.

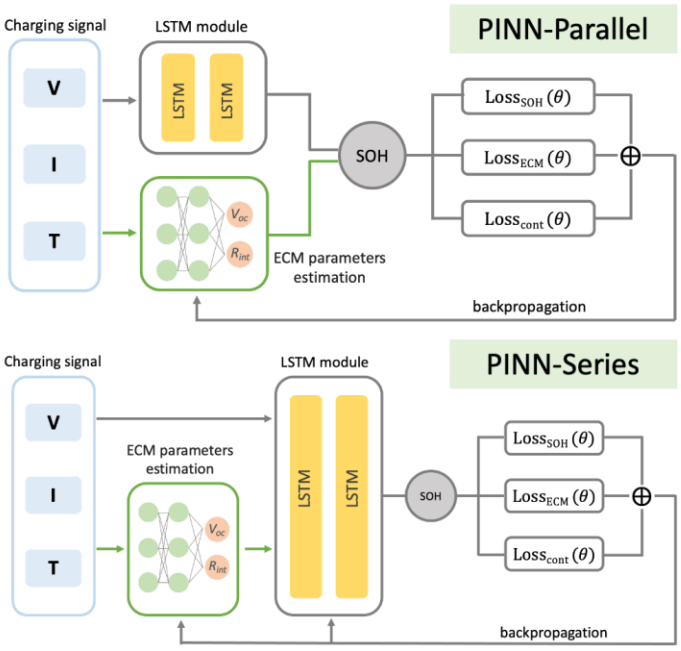

FIGURE 3: STRUCTURE OF PINN-PARALLEL AND PINN-SERIES

3. RESULTS AND DISCUSSION

3.1 Experimental details

In this work, the two PINN models and baseline LSTM model employed for SOH estimation are implemented in Python utilizing the Tensorflow framework. All training and testing procedures are executed and run on a single CPU. The configurations and hyperparameters are empirically determined with the trial-and-error procedure as summarized in Table 1. Consistent hyperparameters are maintained for the single LSTM network and the LSTM components within the two PINNs to ensure a common baseline. This allows performance differences to be attributed directly to architectural variations rather than fine-tuning effectiveness. Future work could explore to identify the optimal configurations for each network.

The LSTM is a simple baseline model without an ECM component, which emphasizes temporal data processing. Alternatively, PINN-Parallel introduces an ECM block that operates in parallel with the LSTM network. This component uses a shared dense layer and different branches for V_{OC} and R_{int} outputs, thus increasing the model's input with physics-informed features. On the other hand, PINN-Series uses a sequential approach to feed the ECM component outputs directly into the LSTM network. This structure provides a deeper integration of physics data into the temporal learning process. Each model employs the Adaptive Moment Estimation (Adam) algorithm to stabilize the training process and minimize the loss

function. Early stopping is implemented throughout the training to mitigate the overfitting and speed up model convergence.

Data from batteries 0006, 0007, and 0018 are used as the training set, while battery 0005 is the test set. All models employ a sliding window of length 10, which means that data from the previous 9 cycles are used to assist in predicting the current state of the battery. In addition to the above standard scenario, the impacts of using less training data and varying lengths of historical information are also explored in Sections 3.4 and 3.5.

The performance of the SOH estimation models is evaluated using two principal statistical measures: Root Mean Square Error (RMSE) and Mean Absolute Error (MAE). RMSE reflects the stability of the model and quantifies its prediction error. MAE serves as a direct indicator to quantify the accuracy of the model. While the PINNs are trained using custom loss functions that incorporate physical constraints and estimations of ECM parameters, the final evaluation of performance is from the SOH prediction. To provide a comparative analysis, all reported model results represent averages from five separate runs.

TABLE 1: MODEL CONFIGURATIONS AND HYPERPARAMETERS

Parameter/ Component	LSTM	PINN-Parallel	PINN-Series
Loss Function	Mean Squared Error	$Loss_{total} = Loss_{SOH} + 0.5\ Loss_{ECM} + 0.5\ Loss_{cont}$ (Equation 11 - 15)	
ECM Component	N/A	Shared layers: 32, 16 (ReLU); V_{OC} branch: 100 (Softplus); R_{int} branch: 100 (Softplus)	
Sliding window size	10		
LSTM Component	128, 64		
Dense Layers to output SOH	32 (ReLU), 1 (Linear)		
Optimizer	Adam (learning rate = 0.001)		
Regularization	Early stopping		
Batch Size	32		
Max. Epochs	1000		

3.2 SOH Prediction Performance

Within the experimental setting outlined in Section 3.1, the SOH predictions from three models are visualized in Figure 4. The RMSE, MAE and training cost are summarized in Figure 5. The PINN-Series and single LSTM demonstrated comparable levels of prediction accuracy, with PINN-Series showing slightly superior performance in terms of lower errors. This modest difference in performance can be attributed to LSTM's tendency for less accurate predictions in the early stages of battery life. As illustrated in Figure 4, the single LSTM model fails to capture the fluctuations in the data during the initial 20 battery cycle predictions. Batteries often behave differently in early cycling than following in their aging patterns due to different dominant degradation mechanisms [30]. A single LSTM model requires a certain amount of data to learn patterns, and early-stage behaviors may not provide sufficiently consistent patterns for the model to capture. The observed better performance of the LSTM model during the middle stage is likely due to its ability to quickly adapt to stable and consistent patterns in this phase. On the other hand, the PINN-Series incorporates knowledge of the underlying physical processes in their architecture. This helps to take into account the different degradation behaviors present in the early cycles. As a result, PINN-Series can provide more accurate representations at this critical stage.

In addition, the PINN-Series has the advantage of a lower standard deviation in different runs, which shows better performance consistency. This suggests that incorporating temporal characteristics of parameters provided by the ECM block can improve the robustness of the model. The PINN-Series could be more consistent in various operational conditions and potentially less sensitive to fluctuations in the data or initial starting conditions of the model. However, the PINN-Parallel shows a reduced accuracy in comparison to the other two. This suggests that the way it uses the output directly from the ECM module instead introduces noise into the model. The evaluation of the validity of ECM output is discussed in Section 3.3.

Despite these advantages, it's important to acknowledge that the additional MLP structure in the PINNs introduces a higher training cost. As shown by the yellow curves in Figure 5, the computational burden for the two PINN models primarily comes from the extra MLP component. The operational cost of an MLP can be influenced by various factors, including the volume of input data. Therefore, the impact of a reduced training dataset and different lengths of history information on model performance should be investigated further.

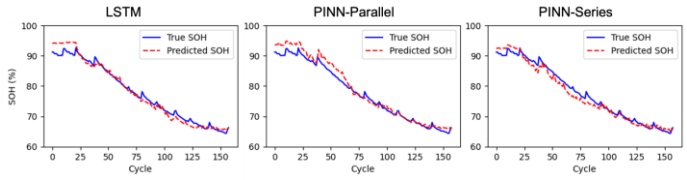

FIGURE 4: SOH PREDICTION PERFORMANCE OF THREE MODELS

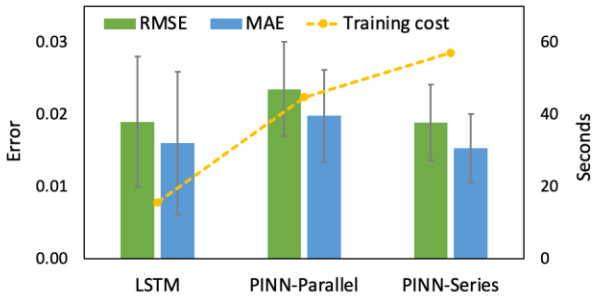

FIGURE 5: RMSE, MAE AND TRAINING COST OF THREE MODELS

3.3 Evaluation of the ECM parameter estimation

The V_{OC} and R_{int} parameters in both the PINN-Parallel and PINN-Series models are estimated using the same MLP network configuration. In addition, these models are trained using the identical customized loss function that combines the SOH prediction error, the ECM parameter estimation error, and the time-continuity constraints on V_{OC} and R_{int}. Since the framework primarily focuses on SOH prediction, this part of the loss is given a higher weight during training to prioritize accuracy.

Figure 6 illustrates the changes in $Loss_{SOH}$ and $Loss_{ECM}$ during the training of PINN-Parallel and PINN-Series. To observe their trends more clearly, 1000 epochs are finished without early stopping. It is shown that the ECM-related losses in both PINN models converge with sufficient training. However, the computation of $Loss_{ECM}$ is based on prediction error of voltage in Equation (12), since real V_{OC} and R_{int} values are difficult to obtain. This indirect optimization implies that even highly precise voltage predictions from the ECM block may not transfer to accurate estimates of V_{OC} and R_{int}.

Figures 7 and 8 present the predictive performance of PINNs for the V, V_{OC} and R_{int} of the same battery cycle in two separate runs. Both models can fit the voltage data well, compatible with the convergence of $Loss_{ECM}$ shown in Figure 6. However, it does not guarantee the fidelity of the V_{OC} and R_{int} simulations. Despite the identical module architecture and inputs, the observed differences in values between parameters in different runs emphasize the stochastic nature of the neural network. This randomness is introduced by the different initial weights and parameters in the training. Therefore, in the absence of reference values for V_{OC} and R_{int}, the ECM part cannot achieve a robust output. Directly utilizing the ECM output for SOH prediction might negatively affect the prediction by introducing noise, as shown in the results of PINN-Parallel.

On the other hand, PINN-Series performs significantly better than PINN-Parallel. This improvement is attributed to PINN-Series learning the temporal characteristics of ECM estimation using LSTM module. As shown in Figure 6, both the two losses are well optimized during training, although the ECM loss decreases more slowly than the SOH one. After about 50 epochs, the SOH loss tends to stabilize while the ECM loss continues to decrease, which shows that the ECM part does not significantly improve the accuracy of the SOH prediction in this standard setup. This was also mentioned in Section 3.2, where PINN-S shows advantages mainly in terms of model stability.

In short, since the ECM component can only indirectly predict V_{OC} and R_{int}, it is not desirable to use these output values directly as physics improvement. However, extracting temporal information from the ECM predicted parameters is more useful. In the case of sufficient training data and appropriate sliding window lengths, the impact on model performance is not obvious, but more on this will be discussed in subsequent sections.

3.4 Influence of limited training data

This section investigates the performance of LSTM and two PINNs on different limited training datasets. Exploring the impact of limited training data is motivated by practical considerations in real-world applications. In many cases, it is time-consuming and costly to collect battery data for a large number of different operating conditions.

Especially for rapidly evolving battery technologies, new chemistries are more likely to encounter a lack of historical data. Therefore, we need to understand the applicability of the models considering the data limitations. In addition, this experiment can evaluate the model's ability to handle overfitting, a common problem when training with limited data. It is critical that models not only fit the training data, but also capture the underlying patterns that can be generalized to new unseen data.

The three models are trained on a combined dataset of batteries 0006, 0007, and 0018, as well as on three individual battery data. The results are summarized in Figure 9. With sufficient training data, all three models demonstrated their best performance. The PINN-Series model consistently shows low error over different training conditions. This model is more capable of dealing with the variability inherent in the different batteries. On the other hand, LSTM shows a more serious overfitting problem when faced with a limited single battery training set.

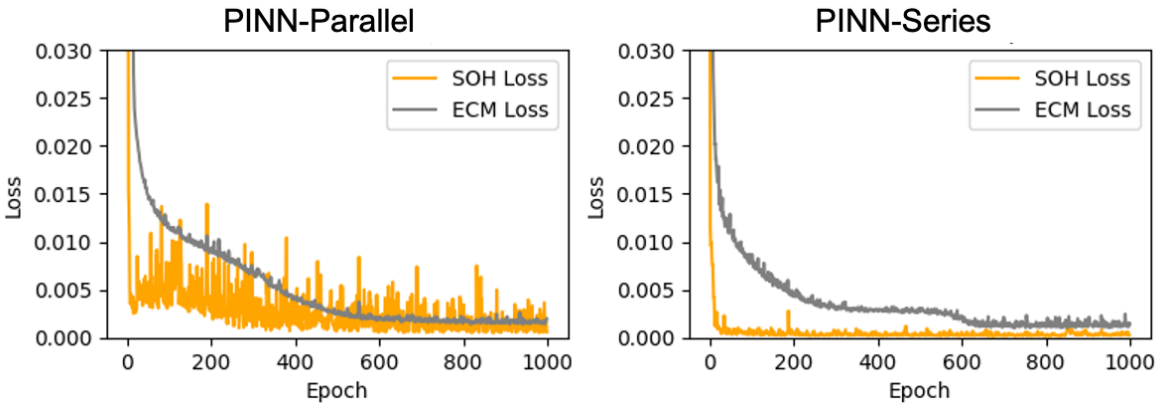

FIGURE 6: TRAJECTORY OF SOH LOSS AND ECM LOSS DURING TRAINING

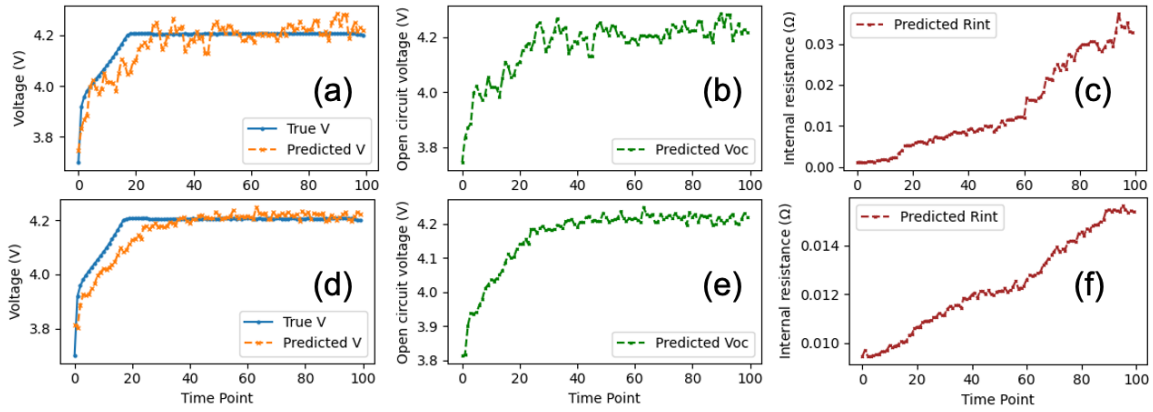

FIGURE 7: PREDICTED VOLTAGE (A/D), OPEN CIRCUIT VOLTAGE (B/E), AND INTERNAL RESISTANCE (C/F) FROM PINN-PARALLEL IN TWO DIFFERENT RUNS

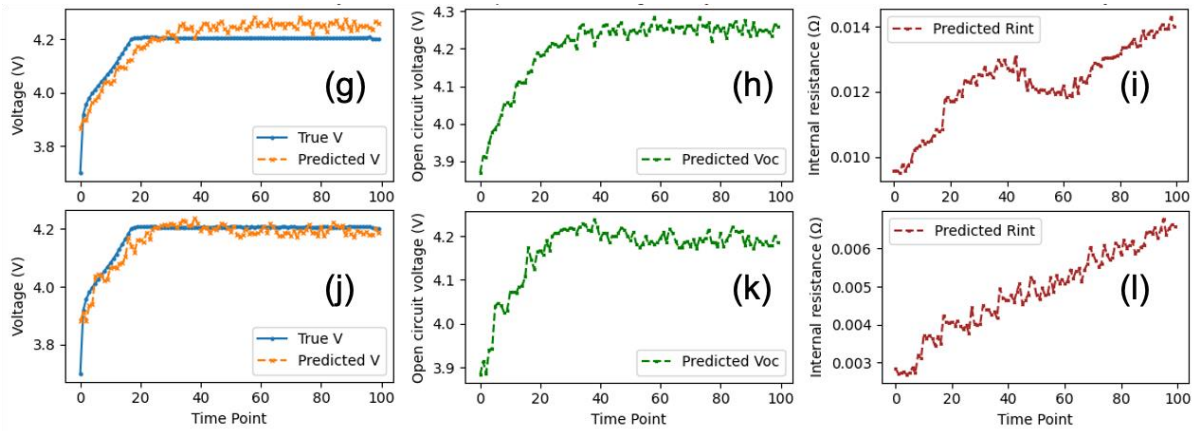

FIGURE 8: PREDICTED VOLTAGE (G/J), OPEN CIRCUIT VOLTAGE (H/K), AND INTERNAL RESISTANCE (I/L) FROM PINN-SERIES IN TWO DIFFERENT RUNS

As seen in Figure 9, LSTM has a relatively low prediction error when trained with battery 0007, which has the most similar degradation trajectory to the test battery observed in Figure 1.

Moreover, with a smaller training set, the running time cost of the two PINNs is reduced by at least 50%. This significantly narrows the gap between their training costs and a single neural network. While the LSTM model is still more computationally efficient, it does not achieve the same level of precision as the two PINN models. Between these two PINN methods, the PINN-Parallel method has a faster training time but compromises prediction accuracy and consistency.

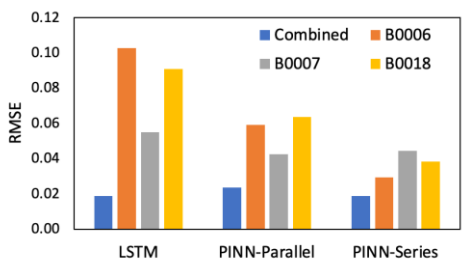

FIGURE 9: MODEL PERFORMANCE OVER DIFFERENT TRAINING SETS

3.5 Influence of Historical Information Length

This section discusses the performance of the three models in predicting SOH under different sliding window sizes. Details of the operation of the sliding window are provided in Section 2.3. The size of the sliding window relates to the length of historical information that can be utilized by the model to make predictions. More historical information can increase the ability of the LSTM block in all three models to capture long-term dependencies. However, if the window is too long, the hidden states in the models may be difficult to capture subtle changes due to information saturation. A long window may allow the LSTM layer to accumulate more noise. More importantly, it would give the model more potential for overfitting as well as a higher computational burden.

The effects of different window sizes varying between 5 to 25 on the model are summarized in Figure 10. The single LSTM model's performance shows variance as the window size increases. This fluctuation in RMSE possibly reflects the overfitting of the LSTM model. Especially with larger window sizes, the model may have learned more noise rather than the underlying pattern. Although PINN-Parallel has physical information involved, its LSTM module is not constrained by the introduced physics. Therefore, the model has the same

deficiency as the single LSTM model when dealing with long windows.

In contrast, the PINN-Series model integrates the laws of physics through the ECM component prior to the LSTM layer and presents greater resistance to overfitting and noise. The loss function in this model restricts the learning process and ensures that the model learns temporal features that adhere to the physical principles. Despite its high training cost, the PINN model achieves consistently high accuracy in SOH prediction. This trend is particularly observable as the window size increases, which means that the model performs well in capturing the temporal dynamics inherent in battery behavior using long historical data. PINN-Series remains the best predictive performer among its competitors, even when historical information is most limited by a window size of 5.

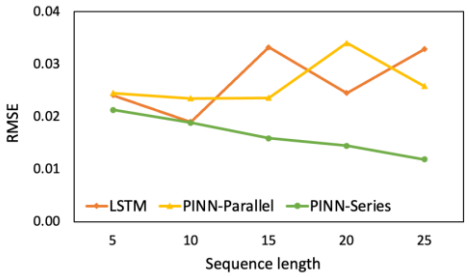

FIGURE 10: MODEL PERFORMANCE OVER DIFFERENT WINDOW SIZE

3.6 Discussion

When comparing the three models, the greatest strength of LSTM is its computational efficiency. With sufficient training data and the proper setting of the sliding window, LSTM can show good prediction accuracy. However, its performance is easily affected by the input data and is prone to overfitting. PINN-Parallel aims to improve predictive performance by incorporating physical features directly into its architecture. However, the ECM module does not provide accurate representations of the internal states. Thus, the parallel architecture may introduce noise instead of features that favor SOH prediction.

The PINN-Series model, with its sequential integration of ECM components into the LSTM network. It learns the temporal patterns and dependencies of these ECM estimations over time, which can be more informative for SOH prediction than the raw ECM outputs themselves. It consistently achieves superior performance with the lowest error and highest robustness. It better handles variability under different battery conditions and also is applicable to cases with limited training data.

PINN-Series requires more training costs than single deep learning networks. However, its robustness shows the potential to run efficiently on smaller training datasets and does not require additional feature engineering. It is worth mentioning that the difference in prediction speed between the trained PINN-Series and the LSTM on the test set is small, with the LSTM being only 10% faster. When deploying pre-trained models, the benefits of the PINN-Series accuracy may outweigh the slight increase in predicting time. This makes the PINN-Series worth considering for tasks where prediction quality is critical.

4. CONCLUSION

In this paper, physics-informed neural networks with different structures are explored for battery state-of-health estimation. The results show that PINN-Series outperforms conventional LSTM and PINN-Parallel models in terms of prediction accuracy and robustness against noise and overfitting. The integration of physical principles through the equivalent circuit model within the LSTM framework improves the model's interpretability and reliability, especially in scenarios with limited training data or varying operational conditions.

While the PINNs present promising results, ongoing research is needed to further refine these models and expand their applicability. The current study utilized a simple Rint model within the framework to represent the battery's internal behavior. Future research could explore the incorporation of more complex ECMs, which may capture the battery dynamics more accurately. Although this may increase the computational complexity, advances in optimization algorithms or data-efficient training strategies can mitigate these challenges. In addition, the significant robustness of the PINN-Series represents the potential to deal with noise and uncertainty in real-world field data. Its usefulness can be tested in future studies.

ACKNOWLEDGEMENTS

This material is based upon work supported by the National Science Foundation–USA under grants # 2324950, and 2324949. Any opinions, findings, conclusions, or recommendations expressed in this material are those of the authors and do not necessarily reflect the views of the National Science Foundation.

REFERENCES

[1] Dai, Q., Kelly, J. C., Gaines, L., and Wang, M., 2019, "Life Cycle Analysis of Lithium-Ion Batteries for Automotive Applications," Batteries, **5**(2), p. 48.

[2] Noura, N., Boulon, L., and Jemeï, S., 2020, "A Review of Battery State of Health Estimation Methods: Hybrid Electric Vehicle Challenges," World Electric Vehicle Journal, **11**(4), p. 66.

[3] Birkl, C., 2017, "Diagnosis and Prognosis of Degradation in Lithium-Ion Batteries," http://purl.org/dc/dcmitype/Text, University of Oxford.

[4] Han, S., Tang, Y., and Khaleghi Rahimian, S., 2021, "A Numerically Efficient Method of Solving the Full-Order Pseudo-2-Dimensional (P2D) Li-Ion Cell Model," Journal of Power Sources, **490**, p. 229571.

[5] S. Edge, J., O'Kane, S., Prosser, R., D. Kirkaldy, N., N. Patel, A., Hales, A., Ghosh, A., Ai, W., Chen, J., Yang, J., Li, S., Pang, M.-C., Diaz, L. B., Tomaszewska, A., Waseem Marzook, M., N. Radhakrishnan, K., Wang, H., Patel, Y., Wu, B., and J. Offer, G., 2021, "Lithium Ion Battery Degradation: What You Need to Know," Physical Chemistry Chemical Physics, **23**(14), pp. 8200–8221.

[6] Jokar, A., Rajabloo, B., Désilets, M., and Lacroix, M., 2016, "Review of Simplified Pseudo-Two-Dimensional Models of Lithium-Ion Batteries," Journal of Power Sources, **327**, pp. 44–55.
[7] Zhang, D., Popov, B. N., and White, R. E., 2000, "Modeling Lithium Intercalation of a Single Spinel Particle under Potentiodynamic Control," J. Electrochem. Soc., **147**(3), p. 831.
[8] Zhang, C., Li, K., Mcloone, S., and Yang, Z., 2014, "Battery Modelling Methods for Electric Vehicles - A Review," *2014 European Control Conference (ECC)*, pp. 2673–2678.
[9] Hu, X., Li, S., and Peng, H., 2012, "A Comparative Study of Equivalent Circuit Models for Li-Ion Batteries," Journal of Power Sources, **198**, pp. 359–367.
[10] Lai, X., Zheng, Y., and Sun, T., 2018, "A Comparative Study of Different Equivalent Circuit Models for Estimating State-of-Charge of Lithium-Ion Batteries," Electrochimica Acta, **259**, pp. 566–577.
[11] He, H., Xiong, R., and Fan, J., 2011, "Evaluation of Lithium-Ion Battery Equivalent Circuit Models for State of Charge Estimation by an Experimental Approach," Energies, **4**(4), pp. 582–598.
[12] Arias Chao, M., Kulkarni, C., Goebel, K., and Fink, O., 2022, "Fusing Physics-Based and Deep Learning Models for Prognostics," Reliability Engineering & System Safety, **217**, p. 107961.
[13] Navidi, S., Thelen, A., Li, T., and Hu, C., 2023, "Physics-Informed Neural Networks for Degradation Diagnostics of Lithium-Ion Batteries," American Society of Mechanical Engineers Digital Collection.
[14] Pang, H., Wu, L., Liu, J., Liu, X., and Liu, K., 2023, "Physics-Informed Neural Network Approach for Heat Generation Rate Estimation of Lithium-Ion Battery under Various Driving Conditions," Journal of Energy Chemistry, **78**, pp. 1–12.
[15] Tian, J., Xiong, R., Lu, J., Chen, C., and Shen, W., 2022, "Battery State-of-Charge Estimation amid Dynamic Usage with Physics-Informed Deep Learning," Energy Storage Materials, **50**, pp. 718–729.
[16] Wang, Y., Han, X., Guo, D., Lu, L., Chen, Y., and Ouyang, M., 2022, "Physics-Informed Recurrent Neural Network With Fractional-Order Gradients for State-of-Charge Estimation of Lithium-Ion Battery," IEEE Journal of Radio Frequency Identification, **6**, pp. 968–971.
[17] Aykol, M., Gopal, C. B., Anapolsky, A., Herring, P. K., Vlijmen, B. van, Berliner, M. D., Bazant, M. Z., Braatz, R. D., Chueh, W. C., and Storey, B. D., 2021, "Perspective—Combining Physics and Machine Learning to Predict Battery Lifetime," J. Electrochem. Soc., **168**(3), p. 030525.
[18] Weddle, P. J., Kim, S., Chen, B.-R., Yi, Z., Gasper, P., Colclasure, A. M., Smith, K., Gering, K. L., Tanim, T. R., and Dufek, E. J., 2023, "Battery State-of-Health Diagnostics during Fast Cycling Using Physics-Informed Deep-Learning," Journal of Power Sources, **585**, p. 233582.
[19] Xu, Z., Guo, Y., and Saleh, J. H., 2022, "A Physics-Informed Dynamic Deep Autoencoder for Accurate State-of-Health Prediction of Lithium-Ion Battery," Neural Comput & Applic, **34**(18), pp. 15997–16017.
[20] Singh, S., Ebongue, Y. E., Rezaei, S., and Birke, K. P., 2023, "Hybrid Modeling of Lithium-Ion Battery: Physics-Informed Neural Network for Battery State Estimation," Batteries, **9**(6), p. 301.
[21] Ye, J., Xie, Q., Lin, M., and Wu, J., 2024, "A Method for Estimating the State of Health of Lithium-Ion Batteries Based on Physics-Informed Neural Network," Energy, **294**, p. 130828.
[22] Fu, H., Liu, Z., Cui, K., Du, Q., Wang, J., and Shi, D., 2024, "Physics-Informed Neural Network for Spacecraft Lithium-Ion Battery Modeling and Health Diagnosis," IEEE/ASME Transactions on Mechatronics, pp. 1–10.
[23] Lin, Y.-H., Ruan, S.-J., Chen, Y.-X., and Li, Y.-F., 2023, "Physics-Informed Deep Learning for Lithium-Ion Battery Diagnostics Using Electrochemical Impedance Spectroscopy," Renewable and Sustainable Energy Reviews, **188**, p. 113807.
[24] "Li-Ion Battery Aging Datasets | NASA Open Data Portal" [Online]. Available: https://data.nasa.gov/dataset/Li-ion-Battery-Aging-Datasets/uj5r-zjdb. [Accessed: 11-Mar-2023].
[25] Su, S., Li, W., Mou, J., Garg, A., Gao, L., and Liu, J., 2023, "A Hybrid Battery Equivalent Circuit Model, Deep Learning, and Transfer Learning for Battery State Monitoring," IEEE Transactions on Transportation Electrification, **9**(1), pp. 1113–1127.
[26] Wang, Y., Xiong, C., Wang, Y., Xu, P., Ju, C., Shi, J., Yang, G., and Chu, J., 2023, "Temperature State Prediction for Lithium-Ion Batteries Based on Improved Physics Informed Neural Networks," Journal of Energy Storage, **73**, p. 108863.
[27] Li, X., Zhang, L., Wang, Z., and Dong, P., 2019, "Remaining Useful Life Prediction for Lithium-Ion Batteries Based on a Hybrid Model Combining the Long Short-Term Memory and Elman Neural Networks," Journal of Energy Storage, **21**, pp. 510–518.
[28] Yang, H., Wang, P., An, Y., Shi, C., Sun, X., Wang, K., Zhang, X., Wei, T., and Ma, Y., 2020, "Remaining Useful Life Prediction Based on Denoising Technique and Deep Neural Network for Lithium-Ion Capacitors," eTransportation, **5**, p. 100078.
[29] Zhang, X., Sun, J., Shang, Y., Ren, S., Liu, Y., and Wang, D., 2022, "A Novel State-of-Health Prediction Method Based on Long Short-Term Memory Network with Attention Mechanism for Lithium-Ion Battery," Frontiers in Energy Research, **10**.
[30] Lv, H., Huang, X., Kang, L., and Liu, Y., 2022, "Quantitative Estimation of Turning Point of Ageing Based on a Two-Stage Model for Lithium-Ion Batteries," J. Electrochem. Soc., **169**(1), p. 010533.

